

A Fast Approach to Segmentation of PET Brain Images for Extraction of Features

Xiaohong Gao ¹, John Clark ²

¹ School of Computing Science, Middlesex University, London, NW4 4BT, United Kingdom

x.gao@mdx.ac.uk

² Wolfson Brain Imaging Centre, University of Cambridge, Cambridge, CB2 2QQ, United Kingdom

jcc24@wbic.cam.ac.uk

Abstract. Position Emission Tomography (PET) is increasingly applied in the diagnosis and surgery in patients thanks to its ability of showing nearly all types of lesions including tumour and head injury. However, due to its natures of low resolution and different appearances as a result of different tracers, segmentation of lesions presents great challenges. In this study, a simple and robust algorithm is proposed via additive colour mixture approach. Comparison with the other two methods including Bayesian classified and geodesic active contour is also performed, demonstrating the proposed colouring approach has many advantages in terms of speed, robustness, and user intervention. This research has many medical applications including pharmaceutical trials, decision making for drug treatment or surgery and patients follow-up and shows potential to the development of content-based image databases when coming to characterise PET images using lesion features.

Keywords: PET imaging, segmentation, additive colour mixture, Lesion detection.

1 Introduction

Positron emission tomography (PET) is an important tool for enabling quantification of human brain function in three dimensions [1]. Through the use of a diverse range of tracers, PET can provide quantitative information on, for example, blood flow, glucose metabolism and neurotransmitter receptor binding potential. However, due to the nature of PET imaging with high noise to signal ratios and its inability of showing anatomic structure, segmentation of lesions, such as head injury and tumour poses great challenge. Due to its many medical applications including pharmaceutical trials, decision making for drug treatment or surgery and patients follow-up, lesion segmentation have been studied extensively by many researchers proposing many promising methods. One group of researchers [2] study the tissue transformation and expansion or contraction effects in order to analysis Multiple Sclerosis (MS) on brain MR images. Mathematical morphological operations have been applied in their study which

are also utilised to delineate lesion regions [3]. Active contour is another popular technique in region detection and boundary delineation, which develops geometric and probabilistic models for shapes and their dynamics in real time. However it suffers the problem of false attraction on noisy images and computational cost [4]. Intelligent mesh algorithm is hence developed by researchers [5] to detect lesion/tumour on CT and Mammography images. Other well known methods for region detection and segmentation include multi-resolution segmentation [6], wavelet based detection [7], texture segmentation [8], and neural network [9]. Multi-resolution scheme has been studied by [10] on the detection of speculated lesions in mammograms, which specifically addresses the difficulty on predetermining the neighbourhood size for feature extraction and fundamentally bases on a linear phase non-separable 2-D wavelet transform.

Conventionally, each method only works well for one particular group of images and performs worse on the other images. At most cases, the methods mentioned above only work well for images with high contrast and low noise. For the images with high noise to signal ratios, such as PET images, most of lesion detection methods do not work well without considerable enhancements.

Statistical methods, for example, Bayes theorem, hence were introduced into this field [11]. Although very promising, Bayesian classified requires large sample data or called training data sets, which sometimes may not be obtained easily. This is due to the fact that different tracer will generate different PET appearance of images for the same subject, resulting different training sets have to be provided.

In this study, a new approach is studied which applies additive colour mixture approach, or called colouring approach, and is under the assumption that a human brain bears similarity with reference of middle plane or middle line in a 2D image form. This approach not only segments lesion robustly but also visualises the lesion in colour, showing an advantage over the other approaches.

2 Methodology

Although most radiological images are in grey scale, colour has been widely introduced in them primarily for the purpose of visualization to increase the contrast between different regions [12]. The most common method is colour map, or a lookup table, by which each colour corresponds to each intensity value in an image. After replacing each pixel with its corresponding colour, the image becomes colourful, generating a pseudo colour image with high contrast.

In some cases, colouring image becomes necessary, especially for fusing multi-modality images, e.g., MR with PET, or CT with PET, to increase high contrast of composite image while maintaining the property of each individual modality. The common method is to colour interleaved pixels using independent colour scales for each modality [13], showing the results of both visually pleasing and easy to interpret.

A colour normally is represented by three independent values, hue, chroma or saturation, and brightness/lightness. Hue is mostly applied in colouring and

contains three primary colours, red, green, and blue. The other hues, i.e., yellow, orange, purple, can be generated by proper mixing of any of these three primary hues (either by mixing coloured lights, e.g. in a computer monitor, or by mixing ink as applied in an ink-jet printer). The mixing procedure can be additive, whereby red, green, and blue are the primary colours (i.e., in a colour monitor), producing white when all three hues of equal part being mixed together. The opposite mixture is subtractive where cyan, magenta and yellow are the primary colours, which is mostly applied in printers in a CMYK colour system (K represents black), producing black colour when mixing all these three primary pigments with equal amounts. Additive colour mixture has been widely applied to viewing medical images and implemented in some open source imaging software including ImageJ(<http://rsb.info.nih.gov/ij/>), which is a convenient way increasing colour contrast. In this study, additive colour mixture technique is investigated to segment lesions of brain PET images.

2.1 Image Colouring

When an image displayed on a computer monitor, one pixel (or voxel in 3D form) can be represented using Red (R), Green (G), Blue (B) colours. For example, in an 8-bits monitor, the intensity range for each colour is 0-255. If all of R, G, and B values are the same for a pixel, this pixel is presented in grey colour, arriving at the intensity value being the average of the sum of these three colour values. As such, other colours can be achieved by the proper mixture of these three primary colours. For example, a yellow pixel can be achieved by the mixture of R, G, and B where B=0, R>0 and G>0, whilst the combination of B>0, R>0 and G=0 will produce a purple colour.

If a 2D brain image with a lesion is represented as I and its reflected image with reference of its middle line as I_R (a flip over image), I and I_R can then be expressed as

$$I = I_L + I_O \quad (1)$$

$$I_R = I_{R_L} + I_{R_O} \quad (2)$$

where L represents lesions in the image, whilst O the rest (other) part of the image. If I is coloured as red as $R(I)$, and I_R green and blue and are represented as $G(I_R)$ and $B(I_R)$ respectively, then

$$R(I) + G(I_R) + B(I_R)$$

$$\begin{aligned} &\Rightarrow R(I_L + I_O) + G(I_{R_L} + I_{R_O}) + B(I_{R_L} + I_{R_O}) \\ &\Rightarrow R(I_L) + R(I_O) + G(I_{R_L}) + G(I_{R_O}) + B(I_{R_L}) + B(I_{R_O}) \\ &\Rightarrow R(I_L) + Cyan(I_{R_L}) + Grey(I_O) \quad (3) \end{aligned}$$

Since a brain image is symmetrical with reference to the middle line (to be discussed below), apart from the lesion part, the rest of brain is more or less the same as its reflected counterparts, resulting $I_O = I_{R_O}$. Therefore the mixture of red, green and blue for the non-lesion pixel would produce grey colour. Similarly the adding of green and blue colour for the reflected lesion region would produce

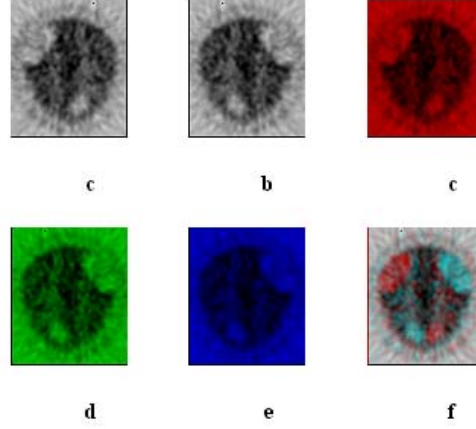


Fig. 1. The procedure of additive colour mixture. From left to right: a). original image, b). reflection of (a), c). (a) in red, d). (b) in green, e). (b) in blue, f). (c) + (d) + (e).

a region with cyan colour. Fig. 1 illustrates the procedure of Eq. (3). The final colour image only contains two colours of red and cyan with one colour associated to the reflected lesion region, i.e., a false region. It is therefore helpful to get rid of that colour first before delineation of lesion boundary. In Fig. 1, the false lesion region is in cyan colour. In order to use meaningful colour attributes instead of RGB space, HSI space is applied in this study to calculate hue, saturation, and intensity values of each pixel. As there are only two hues in the image, it is the saturation attribute that contributes more in processing the image, which is calculated as Eq.(4) [14].

$$H = \arccos \frac{\frac{(R-G)+(R-B)}{2}}{\sqrt{(R-G)^2 + (R-B)(G-B)}} \quad (4)$$

where $H=360^\circ-H$. If $(B/I) > (G/I)$

$$S = 1 - \frac{3\min(R, G, B)}{R + G + B} \quad (5)$$

$$I = \frac{R + G + B}{3} \quad (6)$$

The elimination of cyan colour can then be performed using hue attribute alone. In order to get rid of some red colour that is very close to grey colour, i.e., the background, saturation can be added to the process in addition to hue. For example, the images in Fig. 1 apply 10% saturation as threshold, i.e., any pixel

with less than 10% saturation will be classified as grey colour. It should be noted that the threshold varies according to the tracers applied administrated to the subject, which giving rise to different appearances of PET images and resulting in different thresholds of saturation.

Once an image has only one colour left, a simplified k-mean clustering method is utilised to cluster the lesion region. First, the image is divided into four equal sub-regions (more sub-regions can be generated according to the need). Then the centre of the red colours will be worked out, from which, colour clustering is performed. Then the boundary is delineated using a circular cylinder co-ordinate system with origin located at the centre of the lesion region. When the angle coordinate rotates from 0° to 360° , the radius reached to the edge of the lesion region.

2.2 Locating Middle Line

The success of the above approach depends in some ways on the correctly located symmetrical line of the brain, so that the reflection image with reference to this symmetrical line is similar to the original image apart from the lesion regions.

There are two coordination systems when defining a 3D brain. The *ideal head co-ordinate system* is defined as centred in the brain with positive X_0 , Y_0 , Z_0 axes pointing in the right, anterior and superior direction respectively [15]. With respect to this co-ordinate system, the bilateral symmetry plane of the brain is defined as the plane $X_0 = 0$, passing through the nose. This plane is often referred to as the mid-sagittal plane of the brain. It is expected that a set of axial (coronal) slices is cut perpendicular to the Z_0 (Y_0) axis, and the intersection of each slice with the bilateral symmetry plane appears as a vertical line on the slice [16]. In clinical practice however, a *working co-ordinate system* XYZ is applied. X and Y are oriented along the rows and columns of each image slice, and Z is the actual axis of the scan. The orientation of the working co-ordinate system differs from the ideal co-ordinate system by three rotation angles, *pitch*, *roll* and *yaw*, and three translation differences, ∇X_0 , ∇Y_0 , and ∇Z_0 , respectively.

For each sagittal slice of brain PET image, its left pattern is symmetrical or similar to its right pattern around middle symmetrical line. Hence, its reflection image is similar to the original one. The cross-correction between the original one and the reflected (and rotated) one can then be calculated. The biggest cross-correction (CC) value should be achieved when the corrected rotation angle (θ_j) and translation (c_k) distance are located using Eq. (7).

$$CC(c_k, \theta_j) = \max(\max(XCorr(S_i, rot(2\theta, ref(S_i, c_k)))) \quad (7)$$

where CC is the cross-correlation value, θ_j the yaw angle, and c_k the symmetrical line on the 2D slice S_i . Whilst $ref(S_i, c_k)$ refers to the reflected image of S_i with reference of line at c_k , and *rot* represents rotation. When an image rotates θ degrees, its reflected image rotates 2θ with reference to the original image.

Table 1. The images used in this study with visible lesions (Ls) head injury (HI) and tumour (T).

ID	Diagnosis	No slices	Lesioned slices	Multi-Ls	No detected Ls
1	HI	35	10		10
2	HI	35	5		5
3	HI	70	19		17
4	HI	35	7		7
5	HI	70	24	yes	22
6	HI	70	8		8
7	HI	70	8		8
8	T	69	5	yes	5
9	T	69	15		15
Total		523	101		97

3 Results

Table 1 lists the images studied in this research. One hundred and one slices of 2D images with head injuries and tumors from 9 subjects are collected to evaluate this approach. Although subject number 7 in Table 1 has images with 5 tracers i.e., FDG2D, FDG3D, O15CO2D, O15CO3D, O15water3D, only images with tracer of O15water3D have visible lesions and are included in the study. Similar cases applied to the other subjects. The tumor data are with ^{18}F -FLT (3-Deoxy-3- ^{18}F -fluorothymidine) tracer and are used to study cell proliferation, during which ten subjects are recruited in the ^{18}F -FLT study with two normal subjects as control. Again, only two sets of data are visible and used in our study. Experimental results show that all the lesions are correctly delineated using colouring approach. Figure 2 shows the delineation results for some images with different tracers in-take, showing the appearance of images appears differently. These images have been aligned correctly, i.e., the symmetrical line is in the middle with 0° rotation. Due to the movement of subject, some images are not aligned around the central line. Finding the symmetrical line is then to be performed first as shown in Fig. 3.

Since the edges are delineated using cylinder co-ordinate systems with the scanning line starting from the lesion centre and going from 0° to 360° , some edges may look zigzagged, which is however can be overcome using a smoothing algorithm. After the lesion has been delineated on the rotated and translated image, the delineation of lesions from the original images can then be performed by adding cropping distance and then rotating back the rotated degrees ($-\theta$) obtained during middle line finding.

4 Comparisons

Comparison with two other popular algorithms are made. The first one is Bayesian algorithm and the other is geodesic active contour approach. The Bayesian clas-

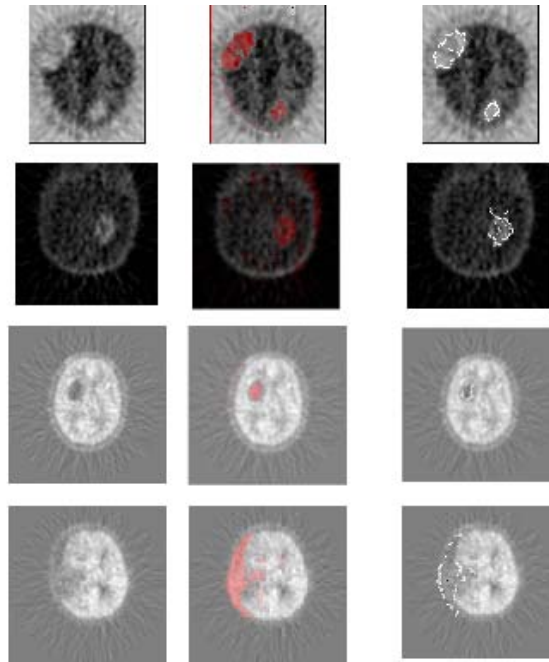


Fig. 2. Delineation results for images. The left column shows the original images, the middle column the images with lesions in red colour, and the right column the lesions with delineated boundary.

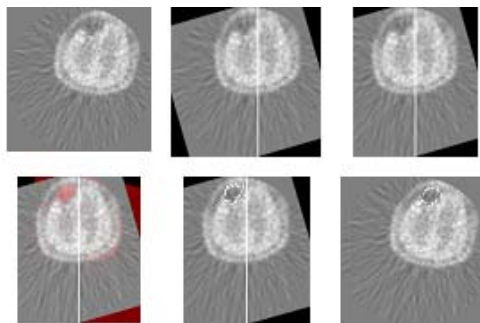


Fig. 3. The steps to from finding symmetrical line to delineating lesion boundary. Top row: (left) original image, (middle) its rotated image with middle line, (right) cropped image from middle. Bottom row: (left) images with coloured lesion region, (middle) edge delineation of lesion region, (right) edge delineation on the original image based on the middle image.

sifier applied in this research is illustrated in Eq.(8).

$$d_i(\bar{x}) = \ln P(C_i) - \frac{1}{2}((\bar{x} - \bar{m}_i)^T C_i^{-1}(\bar{x} - \bar{m}_i)) \quad (8)$$

where $P(C_i)$ is the probability of occurrence of class C_i , $i = 1, 2, \dots, N$, \bar{x} the sample pattern, \bar{m}_i the mean of \bar{x} from C_i , and d_i the decision function. For example, if a pixel is represented as \bar{x} , and $d_i(\bar{x}) > d_j(\bar{x})$, then \bar{x} belongs to class C_i class (e.g., background) rather than C_j (lesions). Sometimes, a error threshold ϵ is introduced to the Eq. (8) so that if $\bar{x} \in C_i$, then

$$d_i(\bar{x}) > d_j(\bar{x}) + \epsilon \quad (9)$$

The second approach studied in this research is geodesic active contour [4], an expansion of snake contour algorithm. To delineate a lesion from 2D PET images, where the lesion corresponds to a region whose pixels are of different grey level intensity, the geodesic contour evolves to the desired boundary according to intrinsic geometry measures of the image. When a user provided an initial guess of the contour (seed), the contour propagates inward or outward in the normal direction driven toward the desired boundaries by image-driven forces. The initial contour should be placed inside the lesions. The final contour is extracted when the evolution stopped. The front contour evolves according to

$$C_t = g(I)((1 - \epsilon k)\bar{N}) - (\nabla g \cdot \bar{N})\bar{N} \quad (10)$$

where level set equation takes form of Eq.(10) to detect boundaries with high differences in their gradient values, as well as small gaps.

$$\phi_t + g_I(1 - \epsilon k)|\nabla\phi| - \beta\nabla P \cdot \nabla\phi = 0 \quad (11)$$

where

$$g_I(x, y) = \frac{1}{1 + |\nabla(G_\sigma * I(x, y))|} \quad (12)$$

which shows that the image $I(x,y)$ convolves with a Gaussian smoothing filter G_σ whose characteristic width is σ . And

$$P(x, y) = -|\nabla(G_\sigma * I(x, y))| \quad (13)$$

which attracts the surface to the edges in the image. Whilst coefficient β in Eq. (11) controls the strength of this attraction. Figure 4 illustrates some comparison results.

On the surface, Fig. 4 shows the delineation results are very much comparable between these three methods. However, for Bayesian approach, the training sets of data will be needed in order to get accurate results, which is not always easy. Different tracers give different appearances of PET images, leading to the requirement of different sets of training data. User intervention will therefore be needed. In Fig. 4, 3rd row, the black dots in the right image represents edges of the lesion detected using Bayesian classifier, whilst the white dots the smoothed

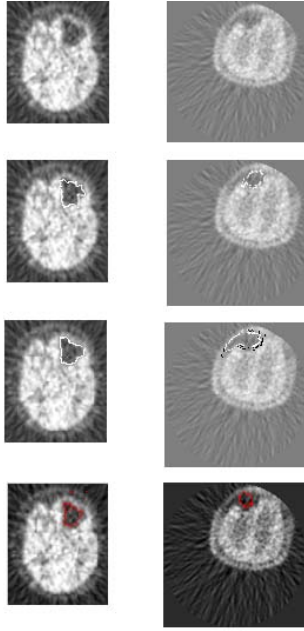


Fig. 4. Comparison results of delineation of lesion using 3 approaches. From top to bottom: original image, the method proposed in the paper, Bayesian classifier, and geodesic active contour.

edge combining the edges of both lesion and the brain. For the data in Table 1, 96% lesions have been delineated accurately using Bayesian classifier, the remaining 4% being the cases with very confusing boundary between lesions and the image background.

As for geodesic active contour approach, seed point is needed from users. Due to the heavy calculation involved, this approach takes much longer than the other two methods (up to a few minutes sometimes). in Fig. 4. Although 100% successful rate has been achieved for delineation of the data given in Table 1, sometimes, the arrived contour is not always the desired boundary.

5 Conclusion and Discussion

In this study, three methods have been studied and compared for lesion delineation, including additive colour mixture, Bayesian classifier, and geodesic contour approaches. Each method has its own pros and cons. Overall, additive colour mixture, or colouring, approach appears to be better in terms of robust, speed, and automation. However, the colouring method has its own limitations. It only applies to the images with symmetry, by which colour adding can then

be applied. For any other images without symmetry, the colour additive mixture can also be utilised as long as there is a template available where the image of interest is registered to spatially.

Acknowledgments. This work is part of TIME (Tele-imaging in Medicine) project funded by European Commission under Asia ICT programme.

References

1. Bendriem, B., Townsend, D.W.(ed.): The Theory and Practice of 3D PET. Kluwer Academic Publishers, London (1998)
2. Thirion, J., Calmon, G.: Measuring Lesion Growth from 3D Medical Images. In: IEEE Workshop on Motion of Non-Rigid and Articulated Objects (NAM '97) (1997) 112–119
3. He, R., Narayana, P.A.: Detection and Delineation of Multiple Sclerosis Lesions in Gadolinium-Enhanced 3D T1-Weighted MRI Data. In: 13th IEEE Symposium on Computer-Based Medical Systems (CBMS) (2000) 201–205
4. Gao, X.W., Birhane, D., Clark, J.: Application of Geodesic Active Contours to the Segmentation of Lesions of PET (Positron Emission Tomography) Images. In: Gao, X., Lin, C, Müller H. (eds.): Medical Imaging and Telemedicine (2005) 45–50
5. Yin, L., Deshpande, S., Chang, J.K.: Automatic Lesion/Tumour Detection Using Intelligent Mesh-Based Active Contour. In: IEEE International Conference on Tools with Artificial Intelligence (ICTAI) (2003)
6. Cai W., Feng D.D., Fulton R.: Content-Based Retrieval of Dynamic PET Functional Images. IEEE Trans. on Info. Tech. in Biome. **4** (2000) 152–158
7. Sawle G.V, Playford E.D., Brooks D.J., Quinn N., Frackowiak R.S.J.: Asymmetrical Pre-synaptic and Post-synaptic Changes in the Striatal Dopamine Projection in Dopa Nave Parkinsonism: Diagnostic Implications of the D2 Receptor Status. Brain. **116** (1993) 853–867
8. Ullmann, J.R: Pattern Recognition Techniques. Crane Russak New York (1973)
9. Lammertsma, A.A., Brench, C.J., Hume S.P., Osman S., Gunn K., Brooks D.J., Frackowiak R.S.: Comparison of Methods for Analysis of Clinical [¹¹C]raclopride Studies. J. Cereb. Blood Flow Metab. **16** (1996) 42–52
10. Liu, S., Babbs, C., and Delp, E.: Multiresolution Detection of Spiculated Lesions in Digital Mammograms. IEEE Trans. on Image Processing **10** (2001) 874–884
11. Huang, C.C., Yu, X., Bading, J., Conti, P.S.: Computer-Aided Lesion Detection with Statistical Model-Based Features in PET Images. IEEE Trans. on Nucl. Science **44** (1997) 2509–2521
12. Ogata, Y., Naito, H., et al.: Novel Display Technique for Reference Images for Visibility of Temporal Change on Radiographs. Radiation Med. **24** (2006) 28–34
13. Rehm, K.R.: Display of Merged Multimodality Brain Images Using Interleaved Pixels with Independent Color Scales. J. Nucl. Med. **35** (1994) 1815–1821
14. Zhao, B.: Colour Space. Computer Vision Laboratory Stony Brook University New York (2002)
15. Talairach, J., Tournoux, P.: Co-Planar Stereotaxic Atlas of the Human Brain. Theme Medical Publishers (1988)
16. Gao, X.W., Batty, S., Clark, J., Fryer, T., Blandford, A.: Extraction of Sagittal Symmetry Planes from PET Images. In: Visualization, Imaging, and Image Processing (VIIP) (2001) 428–433